2023 IEEE International Conference on Bioinformatics and Biomedicine (BIBM) | 979-8-3503-3748-8/23/$31.00 ©2023 IEEE | DOI: 10.1109/BIBM58861.2023.10385846

Modeling of AMPK Regulatory Network in Alzheimer's Disease

Junsheng Wang[1], Enze Xu[2], Yang Xiao[1], Chunrui Xu[3], Minghan Chen[1]
[1]Wake Forest University, {wangj220, xiaoy21, chenm}@wfu.edu
[2]Wake Forest University, {xezpku}@gmail.com
[3]Zhengzhou University, chunruixu@hotmail.com

***Abstract*—AMP-activated protein kinase (AMPK), a cellular energy sensor in response to changes in the ADP/ATP ratio, has been proven to not only play roles in metabolic actions but also holds pivotal roles in neurodegenerative diseases such as Alzheimer's disease (AD), Parkinson's disease, and Lewy body dementia. However, the downstream effectors regulated by AMPK and its specific contributions to the pathology of these diseases remain elusive. In this study, we combine the power of systems biology and neuroscience to understand the dynamics and regulatory effects of AMPK under the progression of AD. Particularly, our study develops a regulatory protein network that seeks to demystify this intricate protein-protein interaction, placing particular emphasis on the role of AMPK in the pathology of AD. By focusing on two important cellular activities, mRNA translation and autophagy, our model explores the underlying effects of the central governance of a change in AMPK activity and concludes that eEF2-controlled translation is more sensitive to the perturbation. Additionally, we adjust various kinetic parameters to restore proteins affected by the disease to their baseline levels, with the goal of identifying potential new drug targets. The model accurately captures the regulatory effect of AMPK, provides the temporal dynamics of key regulators in AD progression, contributes to the understanding of the disease's pathophysiology, and potentially generalizes the function of AMPK into other neurodegenerative diseases.**

I. Introduction

Neurodegenerative diseases, such as Alzheimer's disease (AD), are of mounting concern due to an aging global population and the profound impact these conditions have on quality of life. AD, the predominant cause of dementia, is characterized by progressive cognitive decline, functional impairments, and behavioral changes. Its pathology is marked by the presence of Amyloid β (Aβ) senile plaques, neurofibrillary tangles (NFTs), and neuroinflammation [10]. While Aβ has been one of the focal point of AD research since its identification as a hallmark in 1984, therapeutic interventions targeting its aggregation or enhancing its clearance have not consistently yielded anticipated outcomes. This has prompted a shift in focus towards downstream effectors of Aβ. Notably, AMP-activated protein kinase (AMPK), a metabolic sensor monitoring the ATP to ADP ratio, is emerging as a potential determinant in neurodegenerative processes and may offer a novel avenue for AD therapeutic development [6], [32].

AMPK is a heterotrimeric complex consisting of a catalytic α-subunit and two regulatory β and γ subunit. Several isoforms exist for these subunits (α1, α2; β1, β2; γ1, γ2, γ3), enabling the creation of varied AMPK complexes with unique cellular roles [28]. AMPK is activated in response to stresses that deplete cellular ATP supplies such as low glucose, hypoxia, ischemia, and heat shock. Once the energy deprivation state is detected by AMPK, it switches off the anabolic pathway including fatty acid beta oxidation, fatty acid synthesis, and cholesterol synthesis, and switches on the catabolic pathway by sending more glucose transporter to the cell surface and promoting more glucose intake to generate extra ATP in order to compensate for the energy imbalance [11]. Currently, studies have demonstrated a linkage between the production of neurotoxic Aβ plaque with the oxidative stress that it produces, which ultimately leads to the activation of the AMPK by phosphorylating threonine 172 residue located in the α-subunit activation loop [28]. Numerous cellular activities are modulated by activated AMPK, either directly or through its crosstalk with other pathways. Notably, among these cellular processes, autophagy and mRNA translation are particularly significant potential contributors to the pathology of neurodegenerative diseases and serve as the focal points of our research discussion.

The mammalian target of rapamycin complex (mTORC1) is a central downstream target of AMPK, controlling cell growth, cell proliferation, and survival. An optimal level of mTORC activity is crucial for the survival and function of neuronal cells. However, both excessively high and abnormally low activities can be detrimental to neurons [5]. Autophagy, a cell self-degradation process that eliminates the senile and damaged cell parts, allowing the recycled parts to be utilized as energy sources or as building blocks of the new cell is well controlled by the upregulation of the activated AMPK [5]. While a hypoactive mTROC system may benefit the patient by upregulating the autophagy process to clear out neurotoxic amyloid beta peptide, cells may become desensitized to the AMPK activation signal under prolonged periods. This could reduce the effectiveness of the Aβ-AMPK-autophagy pathway over time. On the other hand, a prolonged hyperactive mTROC system is also detrimental since neurons are generally non-mitotic. Cell cycle machinery is activated while cells do not replicate, causing cellular senescence and ultimately apoptosis. Without further replenishment, the number of available neurons decreases, making it harder for a long-lasting strengthening of synapses between two adjacent neurons [12]. This synaptic strengthening, namely long-term potentiation (LTP), represents a form of neural plasticity and is considered one

of the major cellular mechanisms that underlie forming and retrieving memories.

The other important pathway under AMPK is the eukaryotic elongation factor 2 kinase (eEF2K)—eukaryotic elongation factor 2 (eEF2) pathway. eEF2 is an essential component of the protein synthesis machinery in eukaryotic cells. It plays a pivotal role in the process of translation, specifically during the elongation phase [20]. Extensive studies over the past few decades have established that *de novo* protein synthesis is indispensable for long-lasting forms of synaptic plasticity and memory [2]. AMPK activation modulates eEF2K via two distinct pathways: 1) by suppressing mTORC1 activity, and 2) through the direct phosphorylation of eEF2K, predominantly at the Ser 398 site, a process that operates independently of mTORC1 signaling [4]. Phosphorylated eEF2K phosphorylates eEF2 and inhibits it from protein synthesis (Fig. 1). Experiments have shown that suppression of eEF2K has the ability to correct some of the deficiencies and symptoms brought by AD, and the *de novo* protein synthesis also improves with the suppression. Mass spectrometry analysis revealed that proteins augmented by genetic downregulation of eEF2K play pivotal roles in synaptic functionality, calcium homeostasis, mitochondrial operations, and ATP production. These proteins are instrumental in facilitating LTP and overseeing the structural and functional integrity of dendritic spine morphology [1].

In the complex landscape of Alzheimer's disease, our research focuses on the pivotal role of AMPK and its downstream effectors, mTORC1 and eEF2, which are key regulators of cellular autophagy and mRNA translation, respectively. Utilizing a robust computational model, we aim to establish a quantitative relationship between Aβ and specific cellular activities involved in AD progression. This approach allows us to predict cellular activity changes and propose potential intervention strategies, providing insights into the intricate network of interactions in AD. Our work underscores the significance of AMPK in the diagnostic and therapeutic realm of AD, supported by a rigorous computational model that generates reliable predictions for future experimental work. Ultimately, through this integration of computational modeling and experimental research, our study contributes to a deeper understanding of the mechanisms underpinning AD and the development of more effective diagnostic and treatment strategies.

II. Related Work

The complex interplay of pathways and mechanisms underlying neurodegenerative diseases comes to light, thanks to advancements in molecular biology and neurology. [24] highlight the pivotal role of AMPK activation and its downstream effectors in neurodegenerative diseases, paving the way for further research into potential effectors like Akt, mTORC, S6K1, and others. Building on this, [25] elucidates the intricate balance and connectivity between AMPK activation and mTORC inhibition under different energy stress conditions, and [7] takes the discussion to another level by connecting this signaling pathway with cell biogenesis, regeneration, and autophagy. Another avenue of exploration, as presented in a study [29], concerns the surge in intracellular calcium levels and its subsequent effects on AMPK and mTORC signaling. Additionally, [6] elaborates on the interrelation of AMPK activation with Aβ production and tau phosphorylation. Furthermore, the attenuation of eEF2K activity, influenced substantially by the mTORC complex, AMPK, and MEK/ERK [17], demonstrates potential in mitigating pathophysiological symptoms in AD model mice [1]. Such insights lead us to formulate an AMPK network that integrates the eEF2 and mTORC pathways, intending to enhance our grasp of the mechanisms underpinning AD.

Previously mentioned and other molecular experiments have accumulated abundant data on AMPK regulatory pathways, which provides a broad foundation for mathematically modeling the AMPK-regulated mechanisms of neurodegenerative pathologies. From the structural perspective, [23] demonstrate using both computational prediction and *in vivo* experiment to demonstrate how Aβ and AMPK misfolding contribute to the toxicity of neurodegnerative disease. By modeling the dynamics of regulatory proteins under different conditions, [17] explains the combined interactions of Ca^{2+} and eEF2K in neurons and [25] describes the response to environmental stimuli via AMPK-regulated pathways. The study in [33], [34] provides a meticulous analysis of the vulnerability of individual brain regions by simulating the production, degradation, and diffusion dynamics of AD biomarkers in a spatiotemporal way. Similarly, the research in [19] meticulously crafts a model elucidating synaptic signaling dynamics leading to the activation of AMPK and mTORC across distinct brain subregions. Nevertheless, there has been limited modeling effort directed towards elucidating the regulatory network of AMPK during AD progression. Additionally, insights into protein interactions under varying degrees of AD severity remain relatively scarce.

III. Methodology

In this section, we introduce a protein regulatory framework revolving around AMPK to emulate the dynamic neurodegenerative processes within neural cells. Our objective is to delve into the complex pathology of AD by examining the intricate interplay of proteins and the consequential cellular activities governed by these multifaceted interactions.

A. AMPK regulatory network

Our schematic network begins with the abnormal production of the amyloid precursor protein (APP), which leads to an over-accumulation of amyloid-beta monomers. Through hydrogen bonding, these monomers aggregate into oligomers and plaques, which permeate cerebral cells via multiple receptors. This process results in the activation of AMPK [28], which converts a large proportion of the AMPK into its phosphorylated state (Fig. 1). Subsequently, the activated AMPK governs two interconnected but distinct pathways: the mTROC1 system and the eEF2 pathway. Upon activation, AMPK phosphorylates and activates Tuberous Sclerosis

Complex 2 (TSC2), a crucial component of the TSC protein complex. This complex, also comprised of TSC1, acts as a critical regulator of mTORC1. The TSC complex functions as a GTPase-activating protein (GAP) for the small G-protein Ras homolog enriched in the brain (RHEB). When TSC2 is phosphorylated and activated by AMPK, it enhances the GAP activity of the TSC complex, promoting the conversion of active GTP-bound RHEB to its inactive GDP-bound state. This process decreases the activation level of mTORC1 due to the reduced level of RHEB-GTP [25]. Consequently, the reduced mTORC1 activity leads to a decrease in the phosphorylation of protein phosphatase 2A (PP2A), therefore maintaining more PP2A in its active form. This active PP2A can then dephosphorylate ribosomal protein S6 kinase beta-1 (S6K1) and eEF2K, effectively reducing their activity. On the other side, as a kinase, AMPK directly activates eEF2K, enhancing its activity. eEF2, the only known substrate for eEF2K, is directly phosphorylated by eEF2K. As a result, the mRNA translation rate is diminished due to the decreased availability of eEF2 in its active (dephosphorylated) state [1].

B. Mathematical Model

To illustrate the relative relationship between each pair of protein and their protein modification state, we model each individual protein into two states, either phosphorylated or dephosphorylated state.

$$\text{rate} = \frac{V_{\max} \cdot [S]}{K_m + [S]} \tag{1}$$

The Michaelis-Menten equation is used to model the relationship between a kinase and its substrate [27]. Instead of the regular law of mass equation, the Michaelis-Menten equation describes the saturation behavior of enzymes, as it assumes that there is a finite number of enzyme molecules in the system. As substrate concentration increases, the reaction rate increases but eventually plateaus at $V_{\max}$ reflecting the enzyme's saturation. Also, the Michaelis-Menten equation takes into account the formation of an enzyme-substrate complex, which is often a crucial step in enzyme-catalyzed reactions. On top of that, $V_{\max}$ can be expressed by the product of the turnover number (k_{cat}) and the total enzyme concentration ($[E]_{\text{total}}$). The turnover number, also known as the catalytic constant, represents the maximum number of substrate molecules that an enzyme molecule can convert to a product per unit of time. Thus, the equation is:

$$V_{\max} = k_{\text{cat}} \cdot [E]_{\text{total}} \tag{2}$$

This equation is often used to relate the macroscopic properties of an enzyme-catalyzed reaction (the maximum reaction rate) to its microscopic properties (the turnover number). It assumes that all of the enzymes are in the active form and that the substrate concentration is saturating, which are the conditions under which $V_{\max}$ and k_{cat} are typically measured. Thus, the Michaelis-Menten equation used in our modeling takes the form of

$$\text{rate} = \frac{k_{\text{cat}} \cdot [E]_{\text{total}} \cdot [S]}{K_m + [S]}, \tag{3}$$

where the upper k_{cat} represents in our model to what extent the substrate gets phosphorylated or dephosphorylated by the upstream enzyme. As the value for k_{cat} increases, a greater proportion of the substrate undergoes phosphorylation or dephosphorylation. The lower k_{m} measures the quickness of the reaction completion. As the value for k_{m} increases, the reaction between enzyme and substrate takes a longer time to reach completion.

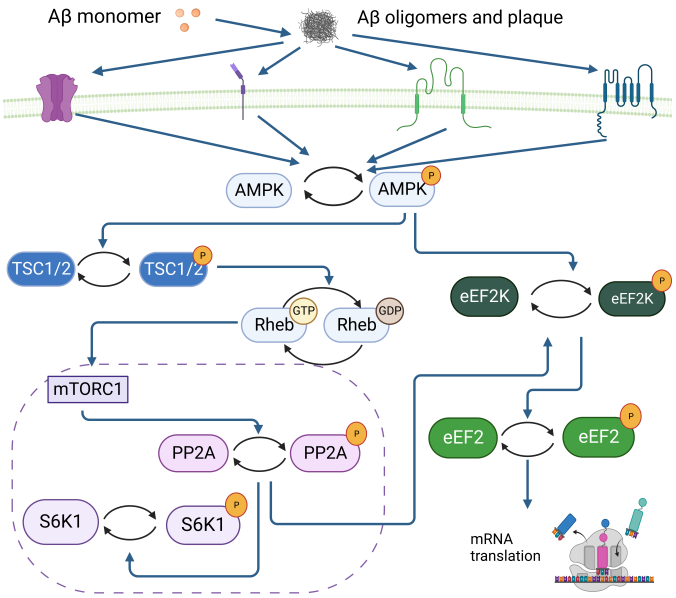

Fig. 1: **Diagram of AMPK-regulated AD pathology.** The protein interaction pathway starts from the accumulation of the extracellular Aβ diffusing into the neuronal cell through different receptors. Activated AMPK regulates two major pathways, mTROC1 and eEF2. (*Created with BioRender.com*)

Based on the proposed mechanistic pathway described in Fig. 1, there is a total of 17 proteins in our model, each represented by an ordinary differential equation that characterizes their respective temporal dynamics. Our model aims to simulate the direct one to one relationship between a kinase and its substrate, thus, neglecting other kinds of ways that may contribute to the change in the state of the substrate. In Table I, take equation (15) as an example, this equation describes the concentration change of phosphorylated state eEF2K as a result of direct phosphorylation by the upstream kinase and dephosphorylation by its phosphatase. The overall rate of change for eEF2K phosphorylation is determined by two main processes. The first is the phosphorylation from eEF2K to peEF2K, which is proportional to the phosphorylation rate constant and the concentration of both activated pAMPK (kinase) and eEF2K (substrate). However, this is offset by

TABLE I: Mathematical Representation for AMPK Regulation Network

(1)	$\frac{d[\mathrm{A}\beta]}{dt} = k_{\mathrm{s\_A}\beta} - k_{\mathrm{d\_A}\beta} \cdot [\mathrm{A}\beta]$
(2)	$\frac{d[\mathrm{AMPK}]}{dt} = -k_{\mathrm{phos\_AMPK}} \cdot \frac{[\mathrm{A}\beta]\cdot[\mathrm{AMPK}]}{K_{\mathrm{phos\_AMPK}}+[\mathrm{AMPK}]} + k_{\mathrm{dephos\_AMPK}} \cdot \frac{[\mathrm{pAMPK}]}{K_{\mathrm{depho\_AMPK}}+[\mathrm{pAMPK}]}$
(3)	$\frac{d[\mathrm{pAMPK}]}{dt} = k_{\mathrm{phos\_AMPK}} \cdot \frac{[\mathrm{A}\beta]\cdot[\mathrm{AMPK}]}{K_{\mathrm{phos\_AMPK}}+[\mathrm{AMPK}]} - k_{\mathrm{dephos\_AMPK}} \cdot \frac{[\mathrm{pAMPK}]}{K_{\mathrm{depho\_AMPK}}+[\mathrm{pAMPK}]}$
(4)	$\frac{d[\mathrm{TSC}]}{dt} = -k_{\mathrm{phos\_TSC}} \cdot \frac{[\mathrm{pAMPK}]\cdot[\mathrm{TSC}]}{K_{\mathrm{phos\_TSC}}+[\mathrm{TSC}]} + k_{\mathrm{dephos\_TSC}} \cdot \frac{[\mathrm{pTSC}]}{K_{\mathrm{depho\_TSC}}+[\mathrm{pTSC}]}$
(5)	$\frac{d[\mathrm{pTSC}]}{dt} = k_{\mathrm{phos\_TSC}} \cdot \frac{[\mathrm{pAMPK}]\cdot[\mathrm{TSC}]}{K_{\mathrm{phos\_TSC}}+[\mathrm{TSC}]} - k_{\mathrm{dephos\_TSC}} \cdot \frac{[\mathrm{pTSC}]}{K_{\mathrm{depho\_TSC}}+[\mathrm{pTSC}]}$
(6)	$\frac{d[\mathrm{Rheb-GTP}]}{dt} = -k_{\mathrm{t2d}} \cdot [\mathrm{pTSC}] \cdot [\mathrm{Rheb-GTP}] + k_{\mathrm{d2t}} \cdot [\mathrm{Rheb-GDP}]$
(7)	$\frac{d[\mathrm{Rheb-GDP}]}{dt} = k_{\mathrm{t2d}} \cdot [\mathrm{pTSC}] \cdot [\mathrm{Rheb-GTP}] - k_{\mathrm{d2t}} \cdot [\mathrm{Rheb-GDP}]$
(8)	$\frac{d[\mathrm{mTORC}]}{dt} = -k_{\mathrm{b\_mTROC}} \cdot [\mathrm{Rheb-GTP}] \cdot [\mathrm{mTORC}] + k_{\mathrm{ub\_mTROC}} \cdot [\mathrm{mTROCa}]$
(9)	$\frac{d[\mathrm{mTORCa}]}{dt} = k_{\mathrm{b\_mTROC}} \cdot [\mathrm{Rheb-GTP}] \cdot [\mathrm{mTORC}] - k_{\mathrm{ub\_mTROC}} \cdot [\mathrm{mTROCa}]$
(10)	$\frac{d[\mathrm{PP2A}]}{dt} = -k_{\mathrm{phos\_PP2A}} \cdot \frac{[\mathrm{mTROCa}]\cdot[\mathrm{PP2A}]}{K_{\mathrm{phos\_PP2A}}+[\mathrm{PP2A}]} + k_{\mathrm{dephos\_PP2A}} \cdot \frac{[\mathrm{pPP2A}]}{K_{\mathrm{depho\_PP2A}}+[\mathrm{pPP2A}]}$
(11)	$\frac{d[\mathrm{pPP2A}]}{dt} = k_{\mathrm{phos\_PP2A}} \cdot \frac{[\mathrm{mTROCa}]\cdot[\mathrm{PP2A}]}{K_{\mathrm{phos\_PP2A}}+[\mathrm{PP2A}]} - k_{\mathrm{dephos\_PP2A}} \cdot \frac{[\mathrm{pPP2A}]}{K_{\mathrm{depho\_PP2A}}+[\mathrm{pPP2A}]}$
(12)	$\frac{d[\mathrm{S6K1}]}{dt} = -k_{\mathrm{phos\_S6K1}} \cdot \frac{[\mathrm{mTROCa}]\cdot[\mathrm{S6K1}]}{K_{\mathrm{phos\_S6K1}}+[\mathrm{S6K1}]} + k_{\mathrm{dephos\_S6K11}} \cdot \frac{[\mathrm{pS6K1}]}{K_{\mathrm{depho\_S6K11}}+[\mathrm{pS6K1}]} + k_{\mathrm{dephos\_S6K12}} \cdot \frac{[\mathrm{PP2A}]\cdot[\mathrm{pS6K1}]}{K_{\mathrm{dephos\_S6K12}}+[\mathrm{pS6K1}]}$
(13)	$\frac{d[\mathrm{pS6K1}]}{dt} = k_{\mathrm{phos\_S6K1}} \cdot \frac{[\mathrm{mTROCa}]\cdot[\mathrm{S6K1}]}{K_{\mathrm{phos\_S6K1}}+[\mathrm{S6K1}]} - k_{\mathrm{dephos\_S6K11}} \cdot \frac{[\mathrm{pS6K1}]}{K_{\mathrm{depho\_S6K1}}+[\mathrm{pS6K1}]} - k_{\mathrm{dephos\_S6K12}} \cdot \frac{[\mathrm{PP2A}]\cdot[\mathrm{pS6K1}]}{K_{\mathrm{dephos\_S6K12}}+[\mathrm{pS6K1}]}$
(14)	$\frac{d[\mathrm{eEF2k}]}{dt} = -k_{\mathrm{phos\_eEF2K}} \cdot \frac{[\mathrm{pAMPK}]\cdot[\mathrm{eEF2k}]}{K_{\mathrm{phos\_eEF2k}}+[\mathrm{eEF2k}]} + k_{\mathrm{dephos\_eEF2k}} \cdot [\mathrm{PP2A}] \cdot \frac{[\mathrm{peEF2k}]}{K_{\mathrm{depho\_eEF2k}}+[\mathrm{peEF2k}]}$
(15)	$\frac{d[\mathrm{peEF2k}]}{dt} = k_{\mathrm{phos\_eEF2K}} \cdot \frac{[\mathrm{pAMPK}]\cdot[\mathrm{eEF2k}]}{K_{\mathrm{phos\_eEF2k}}+[\mathrm{eEF2k}]} - k_{\mathrm{dephos\_eEF2k}} \cdot [\mathrm{PP2A}] \cdot \frac{[\mathrm{peEF2k}]}{K_{\mathrm{depho\_eEF2k}}+[\mathrm{peEF2k}]}$
(16)	$\frac{d[\mathrm{eEF2}]}{dt} = -k_{\mathrm{phos\_eEF2}} \cdot \frac{[\mathrm{peEF2K}]\cdot[\mathrm{eEF2}]}{K_{\mathrm{phos\_eEF2}}+[\mathrm{eEF2}]} + k_{\mathrm{dephos\_eEF2}} \cdot \frac{[\mathrm{peEF2}]}{K_{\mathrm{depho\_eEF2}}+[\mathrm{peEF2}]}$
(17)	$\frac{d[\mathrm{peEF2}]}{dt} = k_{\mathrm{phos\_eEF2}} \cdot \frac{[\mathrm{peEF2K}]\cdot[\mathrm{eEF2}]}{K_{\mathrm{phos\_eEF2}}+[\mathrm{eEF2}]} - k_{\mathrm{dephos\_eEF2}} \cdot \frac{[\mathrm{peEF2}]}{K_{\mathrm{depho\_eEF2}}+[\mathrm{peEF2}]}$

the dephosphorylation of peEF2K back to eEF2K. This dephosphorylation is proportional to the dephosphorylation rate constant and the concentration of both PP2A (phosphatase) and peEF2K (substrate). Equation (1) reflects the change in concentration of Aβ by the mutual effect of synthesis and degradation. Substrates in equation (6,7,8,9) are not subject to phosphorylation; however, they still transition from one activated state to another, represented by the law of mass equations. Other than these, proteins are modeled in a similar way.

A total of 31 parameters (Table II) are used in our mathematical model, with seven parameter values sourced from existing literature and the rest 24 parameter values unknown. We apply the genetic algorithm, specifically the nondominated sorting genetic algorithm (NSGA-II) [26], to optimize the values of unknown parameters. Experimental Western blot data is extracted using ImageJ [9]; each band is extracted four times and the average intensity is used as the final value to smooth out possible discrepancies between each measurement. The relative change between proteins is quantified and used to construct the mathematical equations for the objective function used in the algorithm. The values of unknown parameters are optimized through iterative processes aimed at minimizing the difference between experimental data and simulation, with the final values obtained from the last iteration. A complete list of parameters is provided in Table II, and Table III lists the initial protein concentration at the start of each simulation.

TABLE II: Kinetic Parameters

Parameter	Best Value	Range/Reference
$k_{\mathrm{s\_ab}}$	0.0246	$[5\times10^{-4}, 5\times10^{-1}]$
$k_{\mathrm{d\_ab}}$	0.0376	$[4\times10^{-4}, 4\times10^{-1}]$
$k_{\mathrm{phos\_ampk}}$	0.856	$[5\times10^{-3}, 1]$
$K_{\mathrm{phos\_ampk}}$	635.96	$[12, 800]$
$k_{\mathrm{depho\_ampk}}$	0.2279	$[3\times10^{-4}, 3\times10^{-1}]$
$K_{\mathrm{depho\_ampk}}$	993.84	$[2, 1000]$
$k_{\mathrm{phos\_tsc}}$	6.61×10^{-3}	$[1\times10^{-5}, 2\times10^{-3}]$
$K_{\mathrm{phos\_tsc}}$	1274.99	$[10, 1500]$
$k_{\mathrm{depho\_tsc}}$	6.61×10^{-3}	$[2.3\times10^{-5}, 1\times10^{-2}]$
$K_{\mathrm{depho\_tsc}}$	3896.98	$[80, 6000]$
k_{t2d}	9.746×10^{-5}	$[1.5\times10^{-5}, 3\times10^{-2}]$
k_{d2t}	1.958×10^{-4}	$[1\times10^{-5}, 2\times10^{-3}]$
$k_{\mathrm{b\_mtorc}}$	1.329×10^{-4}	$[4\times10^{-5}, 4\times10^{-3}]$
$k_{\mathrm{ub\_mtorc}}$	4.74×10^{-3}	$[1\times10^{-5}, 7.5\times10^{-3}]$
$k_{\mathrm{depho\_s6k11}}$	3.51×10^{-4}	$[5\times10^{-5}, 5\times10^{-3}]$
$K_{\mathrm{depho\_s6k11}}$	966.456	$[50, 1000]$
$k_{\mathrm{phos\_eef2k}}$	0.0435	$[5\times10^{-5}, 5\times10^{-2}]$
$K_{\mathrm{phos\_eef2k}}$	179.68	$[2, 200]$
$k_{\mathrm{depho\_eef2k}}$	0.0419	$[2.5\times10^{-4}, 5\times10^{-2}]$
$K_{\mathrm{depho\_eef2k}}$	131.2	$[1.5, 150]$
$k_{\mathrm{phos\_eef2}}$	0.01	$[6\times10^{-4}, 3\times10^{-1}]$
$K_{\mathrm{phos\_eef2}}$	15.02	$[0.1, 20]$
$k_{\mathrm{depho\_eef2}}$	0.6457	$[2.3\times10^{-4}, 0.7]$
$K_{\mathrm{depho\_eef2}}$	35.031	$[0.5, 200]$
$k_{\mathrm{phos\_s6k1}}$	2.9×10^{-4}	[17]
$K_{\mathrm{depho\_s6k1}}$	318	[17]
$K_{\mathrm{depho\_s6k12}}$	14.83	[17]
$k_{\mathrm{phos\_pp2a}}$	12	[17]
$K_{\mathrm{phos\_pp2a}}$	46.83	[17]
$k_{\mathrm{depho\_pp2a}}$	30.07	[17]
$K_{\mathrm{phos\_pp2a}}$	22.525	[17]
$k_{\mathrm{depho\_s6k12}}$	0.0012	[17]

IV. Results

A. Dynamics of AMPK-regulated proteins

In this section, we first analyze protein dynamics and interactions. This step ensured that the relative relationships

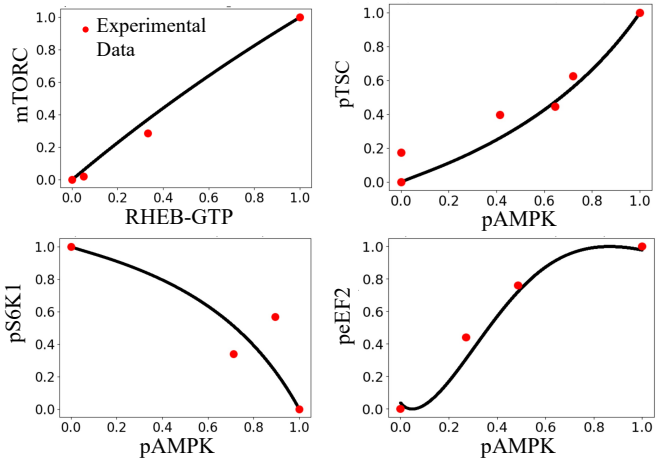

Fig. 2: Comparison between simulated results and experimental data. Solid lines correspond to model outcome, and red dots correspond to experimental data [13], [18], [30], [31].

TABLE III: Cellular Initial State

Protein	Concentration	Protein	Concentration
Aβ	0.5	pPP2A	19.6
AMPk	22.5	pPP2A	19.6
pAMPK	18	S6K1	18
TSC	25	pS6K1	20.5
pTSC	15	eEF2K	44
Rheb-GTP	6.3	peEF2K	23
Rheb-GDP	12.5	eEF2	40
mTROC	60.25	peEF2	16.5
mTROCa	13.5		

between each protein pair evolved as anticipated based on established knowledge. Following this, it was imperative to validate the authenticity of our simulation results. We compared specific protein relationships from our model with experimental data, focusing on the ones between Rheb-GTP with mTORCa, pAMPK with pTSC, pAMPK with pS6K1, and peEF2 with pAMPK, as depicted in Fig. 2.

Both the experimental data, derived from Western blotting, and our simulation outcomes were normalized using the Min-Max scaling, ensuring a consistent range between 0 and 1. As observed in Fig. 2, the simulated data (represented by the black line) closely aligns with the experimental results (indicated by red dots). This congruence underscores the efficacy of our optimization methodology and the accuracy of the constructed protein interaction pathways, ensuring that our subsequent analyses are grounded in robust and validated data, thereby enhancing the reliability and relevance of our findings.

B. eEF2 effect on AD pathology

In our pursuit to elucidate the pathology of AD through kinetic modeling, we meticulously simulated various real-life conditions by modulating kinetic parameters. This approach facilitated a more nuanced understanding of the relative contribution of the mTORC complex and eEF2 to the disease state. We adjusted the kinetic parameter $k_{\text{s\_ab}}$ to 2, 5, and 10-fold of its original level to simulate different levels of neurodegeneration in AD progression, as suggested in [22]. As shown in the left panel of Fig. 3, this led to changes in peEF2 concentration by 8.3%, 14.5%, and 22.3%, respectively, compared to the control group, while the changes in mTORCa concentration were -4.4%, -6.1%, and -7.2%. Meanwhile, we modeled the effect of a hypothetical pAMPK inhibitor by reducing $k_{\text{phos\_AMPK}}$ to 75%, 50%, and 25% of its original level. This yielded changes in peEF2 of -5.2%, -7.8%, and -11.5%, and changes in mTORCa of 2.3%, 3.6%, and 5.2% compared to control.

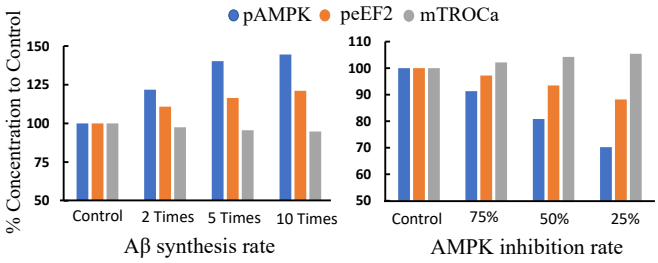

Fig. 3: Percent concentration of three proteins (pAMPK, peEF2, mTROCa) compare to control under different conditions. Left: Simulated results where Aβ synthesis rates increase (2, 5, 10 times respectively) to simulate the different severity of the AD condition. Right: Simulated results of using different AMPK inhibitors to affect the system, where $k_{\text{phos\_AMPK}}$ is reduced to 75, 50, 25 percent of its original level.

These observations underscore a pivotal point: the mTORC pathway, while influential, appears less susceptible to systemic perturbations than the eEF2 pathway. Although both pathways play significant roles in the cellular milieu, the pronounced alterations in peEF2, juxtaposed against mTORCa's more subdued changes, position eEF2-controlled *de novo* protein translation as a more sensitive player in AD's pathology, and it is cogent to postulate that the eEF2 pathway, with its profound influence on protein translation, holds a pivotal role in the pathological cascade of AD [21].

C. Exploration of drug targeting on protein translation

Our model robustly posits that under the influence of Aβ, there is a pronounced perturbation in cellular protein translation, potentially elucidating the underlying pathology of AD. This prediction resonates coherently with many extant experimental data. Notably, studies have documented a discernible decline in protein translation, concomitant with a diminished eEF2 concentration in mutant mice predisposed to aberrant Aβ production [21]. Further corroborating our findings, these empirical investigations have unveiled the therapeutic potential of modulating eEF2 pathways. Specifically, an intriguing experiment involving the crossbreeding of AD genotype mice with eEF2K knockout genotype revealed a salient outcome: the resultant double mutant mice, bereft of the capability

TABLE IV: Therapeutic Target for eEF2

Target pathway	Activity level	Drug type
k_{t2d}	1.467	activator
$k_{\text{ub\_mTROC}}$	Inefficacy	activator
$K_{\text{depho\_ampk}}$	0.283	allosteric activator
$K_{\text{dephos\_pp2a}}$	0.68	allosteric activator
$K_{\text{dephos\_eef2k}}$	0.731	allosteric activator
$K_{\text{dephos\_eef2}}$	0.861	allosteric activator
$k_{\text{dephos\_eef2}}$	1.083	allosteric activator
$k_{\text{dephos\_eef2k}}$	1.251	allosteric activator
$k_{\text{dephos\_pp2a}}$	1.284	allosteric activator
$k_{\text{depho\_ampk}}$	3.376	allosteric activator
$k_{\text{dephos\_TSC}}$	Inefficacy	allosteric activator
$K_{\text{dephos\_TSC}}$	Inefficacy	allosteric activator
$K_{\text{phos\_eef2}}$	1.235	competitive inhibitor
$K_{\text{phos\_eef2k}}$	1.279	competitive inhibitor
$K_{\text{phos\_pp2a}}$	1.355	competitive inhibitor
$K_{\text{phos\_ampk}}$	2.435	competitive inhibitor
$K_{\text{phos\_TSC}}$	Inefficacy	competitive inhibitor
k_{d2t}	0.13	inhibitor
$k_{\text{b\_mTROC}}$	0.744	inhibitor
$k_{\text{phos\_ampk}}$	0.42	non competitive inhibitor
$k_{\text{phos\_pp2a}}$	0.779	non competitive inhibitor
$k_{\text{phos\_eef2k}}$	0.801	non competitive inhibitor
$k_{\text{phos\_eef2}}$	0.9288	non competitive inhibitor
$k_{\text{phos\_TSC}}$	Inefficacy	non competitive inhibitor

to synthesize activated eEF2K, manifested a marked upsurge in protein translation. Concomitantly, there was a discernible alleviation in their AD pathophysiological symptoms in which double mutant mice manifest improved ability in both novel object recognition and old/new object preference task [1]. This empirical evidence underscores the pivotal role of eEF2-centric cellular processes in AD's etiology and illuminates a novel path of inventing potential therapeutics in targeting rescuing the level of protein translation.

In our quest to identify potential therapeutic targets for modulating eEF2 levels and *de novo* protein synthesis, we employed a sensitivity analysis to delineate which model parameters exert the most profound influence on eEF2 concentration. Relevant parameters, implicated in the final concentration of eEF2, are cataloged in Table IV. Depending on their inherent relationship with eEF2 concentration, these parameters are conceptualized as potential targets for either activation or inhibition. In enzymological terms, a competitive inhibitor affects the binding affinity of substrate and enzyme, enlarging the value of the Michealis-Menten constant (K_{m}). A non-competitive inhibitor affects the rate at which substrate is turned into production, thus reducing the turnover number (k_{cat}) in the mathematical equation. An activator serves the opposite as the inhibitor, enhancing k_{cat} as well as reducing K_{m} separately. To ascertain the sensitivity of each parameter, our model aimed for a 10% elevation in eEF2 concentration, subsequently determining the requisite modulation of each parameter to achieve this desired therapeutic outcome. Owing to the bidirectional nature of enzymatic modulation (both enhancement and reduction), normalization was achieved by reciprocally transforming activity levels below unity. In this paradigm, a 10-fold increase or a 10-fold decrease in activity is equated to an equivalent magnitude of change. The less pronounced the required change for a given interaction, the more therapeutically viable it is deemed, thus marking it as a prime candidate for drug targeting [14].

Taking $k_{\text{phos\_eef2}}$ as a paradigmatic example, this parameter governs the interaction between the substrate eEF2 and its upstream kinase peEF2. To attain our therapeutic objective, a diminished conversion rate of eEF2 to peEF2 is sought. As such, the desired modulation necessitates a reduction in the value of $k_{\text{phos\_eef2}}$. In this context, a non-competitive inhibitor emerges as a potent tool. By selectively binding to the allosteric site of peEF2 (the enzyme in this interaction), it can attenuate its catalytic activity, thereby decelerating the conversion of eEF2 (substrate) to its phosphorylated form, peEF2 (product). Model computations elucidate that a diminution to 92.8% of the baseline level of $k_{\text{phos\_eef2}}$ is requisite to instigate a 10% augmentation in eEF2 concentration. The normalized value, 1.0766, underscores the potential of this interaction as a prime therapeutic target. Interestingly, four interactions were delineated as inefficacious within our simulation paradigm. Such interactions either wield a minimal influence, rendering parameter modulation insufficient to realize the desired effect, or their modulation introduces systemic perturbations that inadvertently invert the relational dynamics between specific proteins. Our computational predictions transcend the straightforward targeting of eEF2 and its proximal kinase, eEF2K, offering insights into more intricate upstream interactions that might be therapeutically exploitable. A hierarchy of efficacy is delineated in Fig. 4, with the paramount interactions positioned to the left and the least influential ones to the right.

Remarkably, our analysis unveils that beyond the direct modulation of eEF2, several alternative pathways exhibit comparable therapeutic potential, as evidenced by their capacity to achieve a baseline modification below 150%. This revelation broadens the therapeutic horizon, presenting a multifaceted array of targets. For instance, having discerned the inverse relationship between mTORCa levels and the salutary effects of augmented autophagy, there emerges a compelling proposition: the synthesis of a potent pharmaceutical agent that simultaneously stimulates Aβ autophagy and augments protein translation through the inhibition of mTORCa. In fact, the most well-known mTROC complex inhibitor along with many other inhibitors, have already demonstrated their potency in treating various neurodegenerative diseases, though clinical trials are still limited [3], [16]. Moreover, it's imperative to highlight the apparent suboptimal efficacy of targeting AMPK, a phenomenon that warrants elucidation. As illustrated in Fig. 1, activated AMPK (pAMPK) exerts dual influences. On one flank, it fosters the conversion of eEF2 to peEF2, while conversely, it facilitates the reversion of peEF2 to eEF2 by attenuating the mTORC complex. This dichotomous modulation renders the AMPK pathway less amenable as a sensitive therapeutic target, underscoring the intricacies inherent in cellular signaling networks.

To better illustrate the effectiveness of regulating mTROC rather than AMPK, Fig. 5 provides a simulation of protein

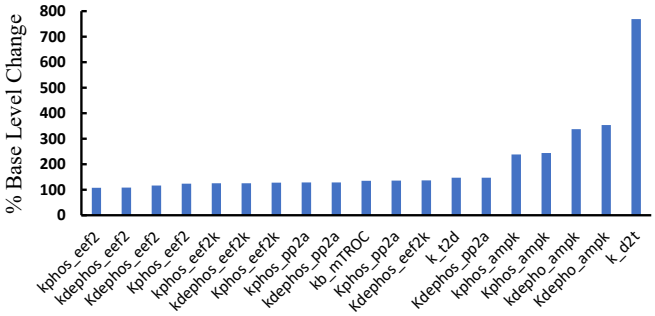

Fig. 4: Simulation illustrating the modulation of specific protein-protein interactions to achieve a desired 10% increase in the final eEF2 concentration. The y-axis refers to the percentage change in parameters relative to their baseline values.

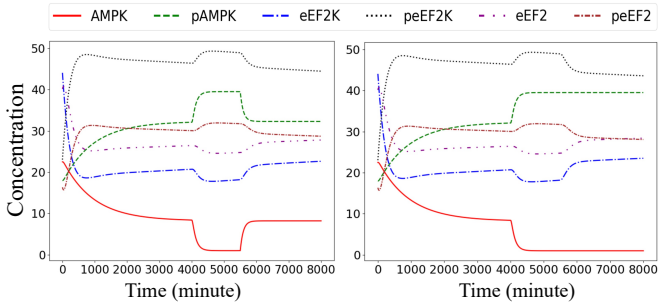

Fig. 5: Simulation illustrating the initiation of AD by enlarging the $k_{\text{s\_ab}}$ by 5-fold at t = 4000 min, followed by either AMPK-targeted or mTROC-targeted medication treatment at t = 5500 min. Left: AMPK-targeted treatment by deactivating AMPK through enlarging $k_{\text{depho\_ampk}}$ by 10-fold. Right: mTROC-targeted treatment by deactivating mTROC through enlarging $k_{\text{ub\_mtorc}}$ by 1.5-fold.

dynamics during the progression of AD with respect to time by either targeting AMPK or mTROC. Initially, the protein system is stabilized to attain its primary equilibrium. Subsequent to this stabilization, AD onset is mimicked by amplifying $k_{\text{s\_ab}}$ by 5-fold at t = 4000 minute. In both figures, we observe the increment in Aβ induces a tremendous activation of AMPK, eEF2K, and a discernible decrease in the activated eEF2 level, contributing to a lower overall protein translation rate. After the system reaches the second equilibrium, to revert these proteins, particularly eEF2, back to their normal state, we simulate targeting either the deactivation of AMPK ($k_{\text{depho\_ampk}}$) or deactivation of mTROC ($k_{\text{ub\_mtorc}}$). Both treatments prove to have a therapeutic effect on reverting proteins eEF2K and eEF2 to their original level, and the only difference is that targeting mTORC complex, a downstream effector of AMPK, does not affect the overall activation level of AMPK, as depicted by the trajectories in red and green in Fig. 5. Though two simulations render comparable therapeutic level, targeting ($k_{\text{depho\_ampk}}$) requires a 10-fold increment, whereas targeting mTROC ($k_{\text{ub\_mtorc}}$) only requires a less than 1.5-fold increment. Once again, this underscores the potential superiority of strategizing interventions on pathways downstream of AMPK for optimal therapeutic leverage.

V. Discussion

In our comprehensive study, we combined systems biology and neuroscience methodologies to construct and validate a regulatory protein network focused on the role of AMPK in AD progression. Our kinetic modeling, rigorously cross-verified against experimental data, unveiled the complex dynamics of protein interactions. Interestingly, while the mTORC pathway emerged as a significant player, it was the eEF2 pathway that stood out, revealing its paramount role in AD's pathological cascade. Sensitivity analyses further spotlighted potential therapeutic targets, emphasizing the therapeutic potential of modulating eEF2 levels and *de novo* protein synthesis. These insights set the stage for exploring innovative therapeutic interventions, particularly those targeting the pivotal eEF2-centric cellular processes.

While our study offers invaluable insights into the intricate protein interactions in AD progression, we recognize some inherent limitations. Firstly, our model, despite being robust, is a simplification of the highly complex biological processes. As such, some nuance interactions of feedback loop and the complex crosstalk between pathways might not be fully represented. For instance, the tau hyperphosphorylation cascade, another critical hallmark in AD, is regulated by various feedback mechanisms through glycogen synthase kinase 3β (GSK-3β) and cyclin-dependent kinase 5 (CDK5) [15]. Additionally, the amyloid precursor protein (APP) processing pathway, which results in the production of Aβ peptides, possesses intricate feedback loops that can influence Aβ production rates. Future studies can incorporate more elements by building on the existing model, mapping out a bigger picture of AD, and allowing a more comprehensive exploration of the multifaceted interactions and regulatory mechanisms inherent in the disease's progression. Secondly, the parameter values utilized in our model, though rigorously optimized, are derived from existing literature and experimental data. These values might not fully capture the diverse variability inherent in *in vivo* conditions. Authenticating our findings through wet lab validation would significantly enhance the authenticity of our results and bolster the predictive capability of the model.

Understanding the intricacies of protein translation extends beyond just the realm of Alzheimer's disease; it encompasses a broader spectrum of neurodegenerative diseases. The delicate equilibrium of protein translation is not merely pivotal for synaptic plasticity and neuronal functionality but also underpins cellular growth, differentiation, and the cellular response to various stressors. Disruptions in this crucial balance have repercussions that manifest in a slew of neurodegenerative conditions, from Parkinson's disease and Huntington's disease to amyotrophic lateral sclerosis (ALS) [8]. While direct inter-

ventions targeting eEF2 have demonstrated therapeutic potential in various *in vivo* animal studies, the translation of these findings into clinical practice remains embryonic. As of now, clinical trials specifically targeting eEF2 are conspicuously absent, underscoring the nascent stage of this research avenue. Conversely, strategies aimed at inhibiting mTORC, which our study suggests can emulate the therapeutic effects of eEF2 modulation, are already in the clinical trial pipeline, with some advancing to early phase I and II stages. Thus, our findings, combined with the success of targeting mTORC in clinical trials, underscore the urgent need for dedicated research into drugs that target eEF2, offering potential therapeutic avenues for various neurodegenerative disorders.

REFERENCES

[1] B. C. Beckelman, W. Yang, N. P. Kasica, H. R. Zimmermann, X. Zhou, C. D. Keene, A. G. Ryazanov, T. Ma *et al.*, "Genetic reduction of eef2 kinase alleviates pathophysiology in alzheimer's disease model mice," *The Journal of clinical investigation*, vol. 129, no. 2, pp. 820–833, 2019.

[2] D. Bochicchio, L. Christie, C. Lawrence, K. Herholz, C. Parker, R. Hinz, and H. Boutin, "Measurement of protein synthesis rate in rat by [11c] leucine pet imaging: Application to the tgf344-ad model of alzheimer's disease," *Molecular Imaging and Biology*, vol. 25, no. 3, pp. 596–605, 2023.

[3] J. Bové, M. Martínez-Vicente, and M. Vila, "Fighting neurodegeneration with rapamycin: mechanistic insights," *Nature Reviews Neuroscience*, vol. 12, no. 8, pp. 437–452, 2011.

[4] G. J. Browne, S. G. Finn, and C. G. Proud, "Stimulation of the amp-activated protein kinase leads to activation of eukaryotic elongation factor 2 kinase and to its phosphorylation at a novel site, serine 398," *Journal of Biological Chemistry*, vol. 279, no. 13, pp. 12 220–12 231, 2004.

[5] Z. Cai, G. Chen, W. He, M. Xiao, and L.-J. Yan, "Activation of mtor: a culprit of alzheimer's disease?" *Neuropsychiatric disease and treatment*, pp. 1015–1030, 2015.

[6] Z. Cai, L.-J. Yan, K. Li, S. H. Quazi, and B. Zhao, "Roles of AMP-activated protein kinase in Alzheimer's disease," *Neuromolecular medicine*, vol. 14, pp. 1–14, 2012.

[7] B. Carroll and E. A. Dunlop, "The lysosome: a crucial hub for ampk and mtorc1 signalling," *Biochemical Journal*, vol. 474, no. 9, pp. 1453–1466, 2017.

[8] G. Cestra, S. Rossi, M. Di Salvio, and M. Cozzolino, "Control of mrna translation in als proteinopathy," *Frontiers in molecular neuroscience*, vol. 10, p. 85, 2017.

[9] G. Gallo-Oller, R. Ordonez, and J. Dotor, "A new background subtraction method for western blot densitometry band quantification through image analysis software," *Journal of immunological methods*, vol. 457, pp. 1–5, 2018.

[10] P. Gehlot, S. Kumar, V. K. Vyas, B. S. Choudhary, M. Sharma, and R. Malik, "Guanidine-based β amyloid precursor protein cleavage enzyme 1 (BACE-1) inhibitors for the Alzheimer's disease (AD): A Review," *Bioorganic & Medicinal Chemistry*, p. 117047, 2022.

[11] D. Hardie, "AMPK: a key regulator of energy balance in the single cell and the whole organism," *International journal of obesity*, vol. 32, no. 4, pp. S7–S12, 2008.

[12] F. E. Henry, A. J. McCartney, R. Neely, A. S. Perez, C. J. Carruthers, E. L. Stuenkel, K. Inoki, and M. A. Sutton, "Retrograde changes in presynaptic function driven by dendritic mtorc1," *Journal of Neuroscience*, vol. 32, no. 48, pp. 17 128–17 142, 2012.

[13] S. Horman, C. Beauloye, D. Vertommen, J.-L. Vanoverschelde, L. Hue, and M. H. Rider, "Myocardial ischemia and increased heart work modulate the phosphorylation state of eukaryotic elongation factor-2," *Journal of Biological Chemistry*, vol. 278, no. 43, pp. 41 970–41 976, 2003.

[14] B. Ingalls, "Sensitivity analysis: from model parameters to system behaviour," *Essays in biochemistry*, vol. 45, pp. 177–194, 2008.

[15] K. Iqbal, F. Liu, C.-X. Gong, and I. Grundke-Iqbal, "Tau in alzheimer disease and related tauopathies," *Current Alzheimer Research*, vol. 7, no. 8, pp. 656–664, 2010.

[16] M. Kaeberlein and V. Galvan, "Rapamycin and alzheimer's disease: time for a clinical trial?" *Science translational medicine*, vol. 11, no. 476, p. eaar4289, 2019.

[17] J. W. Kenney, O. Sorokina, M. Genheden, A. Sorokin, J. D. Armstrong, and C. G. Proud, "Dynamics of elongation factor 2 kinase regulation in cortical neurons in response to synaptic activity," *Journal of Neuroscience*, vol. 35, no. 7, pp. 3034–3047, 2015.

[18] M. Kim and J. H. Lee, "Identification of an ampk phosphorylation site in drosophila tsc2 (gigas) that regulate cell growth," *International journal of molecular sciences*, vol. 16, no. 4, pp. 7015–7026, 2015.

[19] A. Leung and P. Rangamani, "Computational modeling of ampk and mtor crosstalk in glutamatergic synapse calcium signaling," *npj Systems Biology and Applications*, vol. 9, no. 1, p. 34, 2023.

[20] J. K. Lim, A. Samiei, C. J. Carnie, V. Brinkman, D. Radiloff, J. Cran, G. Leprivier, and P. H. Sorensen, "The eEF2 kinase coordinates the DNA damage response to cisplatin by supporting p53 activation," *bioRxiv*, pp. 2023–03, 2023.

[21] T. Ma, "Roles of eukaryotic elongation factor 2 kinase (eef2k) in neuronal plasticity, cognition, and alzheimer disease," *Journal of Neurochemistry*, 2021.

[22] P. Mao, M. Manczak, M. J. Calkins, Q. Truong, T. P. Reddy, A. P. Reddy, U. Shirendeb, H.-H. Lo, P. S. Rabinovitch, and P. H. Reddy, "Mitochondria-targeted catalase reduces abnormal app processing, amyloid β production and bace1 in a mouse model of alzheimer's disease: implications for neuroprotection and lifespan extension," *Human Molecular Genetics*, vol. 21, no. 13, pp. 2973–2990, 2012.

[23] P. H. Nguyen, A. Ramamoorthy, B. R. Sahoo, J. Zheng, P. Faller, J. E. Straub, L. Dominguez, J.-E. Shea, N. V. Dokholyan, A. De Simone *et al.*, "Amyloid oligomers: A joint experimental/computational perspective on alzheimer's disease, parkinson's disease, type ii diabetes, and amyotrophic lateral sclerosis," *Chemical reviews*, vol. 121, no. 4, pp. 2545–2647, 2021.

[24] C. A. Peixoto, W. H. de Oliveira, S. M. da Racho Araújo, and A. K. S. Nunes, "Ampk activation: Role in the signaling pathways of neuroinflammation and neurodegeneration," *Experimental neurology*, vol. 298, pp. 31–41, 2017.

[25] M. Sadria and A. T. Layton, "Interactions among mtorc, ampk and sirt: a computational model for cell energy balance and metabolism," *Cell Communication and Signaling*, vol. 19, no. 1, pp. 1–17, 2021.

[26] W. Sheng, K.-Y. Liu, Y. Liu, X. Meng, and Y. Li, "Optimal placement and sizing of distributed generation via an improved nondominated sorting genetic algorithm ii," *IEEE Transactions on power Delivery*, vol. 30, no. 2, pp. 569–578, 2014.

[27] B. Srinivasan, "A guide to the michaelis–menten equation: steady state and beyond," *The FEBS journal*, vol. 289, no. 20, pp. 6086–6098, 2022.

[28] V. Vingtdeux, P. Davies, D. W. Dickson, and P. Marambaud, "Ampk is abnormally activated in tangle-and pre-tangle-bearing neurons in alzheimer's disease and other tauopathies," *Acta neuropathologica*, vol. 121, pp. 337–349, 2011.

[29] V. Vingtdeux, L. Giliberto, H. Zhao, P. Chandakkar, Q. Wu, J. E. Simon, E. M. Janle, J. Lobo, M. G. Ferruzzi, P. Davies *et al.*, "Amp-activated protein kinase signaling activation by resveratrol modulates amyloid-β peptide metabolism," *Journal of Biological Chemistry*, vol. 285, no. 12, pp. 9100–9113, 2010.

[30] A. Wani, S. B. Al Rihani, A. Sharma, B. Weadick, R. Govindarajan, S. U. Khan, P. R. Sharma, A. Dogra, U. Nandi, C. N. Reddy *et al.*, "Crocetin promotes clearance of amyloid-β by inducing autophagy via the stk11/lkb1-mediated ampk pathway," *Autophagy*, vol. 17, no. 11, pp. 3813–3832, 2021.

[31] H. Yang, X. Jiang, B. Li, H. J. Yang, M. Miller, A. Yang, A. Dhar, and N. P. Pavletich, "Mechanisms of mtorc1 activation by rheb and inhibition by pras40," *Nature*, vol. 552, no. 7685, pp. 368–373, 2017.

[32] L. Yang, Y. Jiang, L. Shi, D. Zhong, Y. Li, J. Li, and R. Jin, "Ampk: potential therapeutic target for alzheimer's disease," *Current Protein and Peptide Science*, vol. 21, no. 1, pp. 66–77, 2020.

[33] J. Zhang, Q. Liu, H. Zhang, M. Dai, Q. Song, D. Yang, G. Wu, and M. Chen, "Uncovering system vulnerability and criticality of human brain under evolving neuropathological events in alzheimer's disease," *arXiv preprint arXiv:2201.08941*, 2022.

[34] J. Zhang, D. Yang, W. He, G. Wu, and M. Chen, "A network-guided reaction-diffusion model of at [n] biomarkers in alzheimer's disease," in *2020 IEEE 20th International Conference on Bioinformatics and Bioengineering (BIBE)*. IEEE, 2020, pp. 222–229.